



This discussion paper is/has been under review for the journal Natural Hazards and Earth System Sciences (NHESD). Please refer to the corresponding final paper in NHESD if available.

Seismology of the Oso-Steelhead landslide

C. Hibert, C. P. Stark, and G. Ekström

Lamont-Doherty Earth Observatory, Columbia University, Palisades, NY, USA

Received: 12 November 2014 – Accepted: 17 November 2014 – Published: 5 December 2014

Correspondence to: C. Hibert (hibert@ldeo.columbia.edu)

Published by Copernicus Publications on behalf of the European Geosciences Union.

NHESD

2, 7309–7327, 2014

Seismology of the Oso-Steelhead landslide

C. Hibert et al.

Title Page

Abstract

Introduction

Conclusions

References

Tables

Figures



Back

Close

Full Screen / Esc

Printer-friendly Version

Interactive Discussion



Abstract

We carry out a combined analysis of the short- and long-period seismic signals generated by the devastating Oso-Steelhead landslide that occurred on 22 March 2014. The seismic records show that the Oso-Steelhead landslide was not a single slope failure, but a succession of multiple failures distinguished by two major collapses that occurred approximately three minutes apart. The first generated long-period surface waves that were recorded at several proximal stations. We invert these long-period signals for the forces acting at the source, and obtain estimates of the first failure runout and kinematics, as well as its mass after calibration against the mass-center displacement estimated from remote-sensing imagery. Short-period analysis of both events suggests that the source dynamics of the second are more complex than the first. No distinct long-period surface waves were recorded for the second failure, which prevents inversion for its source parameters. However, by comparing the seismic energy of the short-period waves generated by both events we are able to estimate the volume of the second. Our analysis suggests that the volume of the second failure is about 15–30% of the total landslide volume, which is in agreement with ground observations.

1 Introduction

On 22 March 2014, a catastrophic landslide occurred 6.4 km east of Oso (Washington, USA), destroying the neighborhood known as “Steelhead Haven” and causing 43 fatalities. The failure occurred on a slope which had already been affected by at least six episodes of collapse since 1955. It was preceded by several days of heavy rainfall.

The landslide traveled approximately 1.1 km and separated into two segments. The majority of the mobilized material accumulated in the western segment. Deposits of the landslide formed a dam on the north fork of the Stillaguamish river. Ground observations suggest a total volume of the deposits of approximately $7.6 \times 10^6 \text{ m}^3$ (Keaton et al., 2014).

Seismology of the Oso-Steelhead landslide

C. Hibert et al.

Title Page

Abstract

Introduction

Conclusions

References

Tables

Figures



Back

Close

Full Screen / Esc

Printer-friendly Version

Interactive Discussion



Seismology of the Oso-Steelhead landslide

C. Hibert et al.

Title Page	
Abstract	Introduction
Conclusions	References
Tables	Figures
◀	▶
◀	▶
Back	Close
Full Screen / Esc	
Printer-friendly Version	
Interactive Discussion	



Reconstructing the failure sequence of a landslide mass is a challenging task, as direct observations of the mass movements are rare. In recent years, seismology has proven useful in this regard by offering a way to infer the dynamics of large mass movements (e.g., Brodsky et al., 2003; Favreau et al., 2010; Schneider et al., 2010; Moretti et al., 2012; Yamada et al., 2013; Allstadt, 2013) and estimate important properties such as the mobilized mass (Ekström and Stark, 2013). Additional analysis of the short-period waves provides an extra constraint on source mechanisms and a more complete understanding of the dynamics of slope failures (e.g., Suriñach et al., 2005; Deparis et al., 2008; Vilajosana et al., 2008; Dammeier et al., 2011; Hibert et al., 2011, 2014).

In this study we present a joint interpretation of the long-period force history of the Oso-Steelhead landslide and the associated short-period seismic signals. Our study builds on and extends the ground observations and results presented in the Geotechnical Extreme Events Reconnaissance report by Keaton et al. (2014). We first discuss the seismic observations made on short-period and broadband stations, which indicate that two consecutive slope failures occurred. We then present the results of the inversion of the landslide force history (LFH) of the long-period signals generated by the first landslide, and provide an estimate of its mass, peak velocity and acceleration. Finally we compare the short-period seismic signals to the LFH, which leads to interpretations on the dynamics of the first landslide. We also discuss, based on a comparison of the seismic records and with reference to the ground observations, the possible source characteristics of the second event.

2 Seismic observations

The seismic waves generated by the Oso-Steelhead landslide were recorded by several short-period and broadband stations (Fig. 1). Two high-amplitude short-period signals were recorded on stations at distances ranging from 11.7 to 180 km. The first strong seismic signal onset was recorded at 17:37:22 UTC on the closest short-period

station (JCW) from the Pacific Northwest Regional Seismic Network (FDSN network code UW), at a distance of 11.7 km. The short-period (1–10 Hz) seismic signal recorded at JCW has a duration of 120 s, and exhibits all the known features of landslide-generated seismic signals: emergent onset, no distinct P and S waves and no clear peak amplitude visible in the higher-frequency bands (Fig. 2a and b) (Suriñach et al., 2005; Deparis et al., 2008; Dammeier et al., 2011; Hibert et al., 2011). Spectral analysis of the seismic signal recorded at JCW shows persistent high energy between 1 and 10 Hz (Fig. 2c), remaining high for approximately one minute before a gradual decay.

A second event was recorded at 17:41:53 at JCW. Its signal has a more impulsive onset than that of the first event and a shorter duration of 60 s. It exhibits several consecutive amplitude peaks in the 1–3 Hz frequency band (Fig. 2a). The onset of the seismic signal of the second event is marked by a strong burst of energy in the 3–10 Hz band (Fig. 2b). A second burst of energy in this frequency band is observed at the end of the signal (Fig. 2b and c). The two peaks following the onset and observed in the 1–3 Hz band do not appear in the 3–10 Hz frequency band (Fig. 3). On the closest stations, several other weak but distinct short-period signals were recorded (e.g., at 17:43:30 – Fig. 3b) that were possibly generated by residual collapses in the hours following as a result of local destabilization caused by the two main events.

Long-period surface waves ($T < 30$ s) were also detected for the first event (Fig. 2d) at five broadband stations (four from the USArray Transportable Array), with distances from the landslide ranging from 18.3 to 140.8 km. No distinct long-period seismic signal was observed for the second event (Fig. 2d). Several differences between the seismic signals of the two events are therefore identified: (1) the seismic signal of the second event has a more impulsive onset than the first (Fig. 2a and b), (2) several distinct amplitude peaks are observed in the signal of the second event filtered in the 1–3 Hz frequency and not for the first event (Fig. 2a), (3) the seismic signal of the second event has less energy in the frequency band above 5 Hz compared to the first (Fig. 2c), (4) a strong long-period signal was generated by the first event, and absent for the second. These observations suggest differences in the dominant source characteristics.

NHESSD

2, 7309–7327, 2014

Seismology of the Oso-Steelhead landslide

C. Hibert et al.

Title Page

Abstract

Introduction

Conclusions

References

Tables

Figures



Back

Close

Full Screen / Esc

Printer-friendly Version

Interactive Discussion



3 Landslide force history

The acceleration and deceleration of the bulk mass during the landslide cause a loading and unloading of the slope that generates long-period seismic waves. The forces acting on the slide mass that bring about this loading-unloading cycle are gravity, basal friction, and centripetal forces, and each of these has a reactive counterpart acting on the solid earth in the opposite direction across the slide contact area. The landslide therefore exerts a force F on the solid Earth that is the vector opposite of the force F_S , equivalent to the bulk momentum change of the slide

$$F[\mathbf{x}, t] = -F_S = -\frac{d(m\mathbf{v})}{dt}[\mathbf{x}, t]. \quad (1)$$

The time-varying forces acting on the slope during the loading-unloading cycle can be retrieved by inversion of long-period seismic waves, and thereby provide a force history from which information on the dynamics of the landslide can be inferred.

We use the inversion method developed by Ekström and Stark (2013) to determine the Landslide Force History (LFH) of the Oso-Steelhead landslide from the long-period waveforms recorded at five broadband stations. The method is based on the approximation that, when considering the long-period signals, the landslide seismic source can be described as a time-varying, 3-D force vector acting at a fixed point (Kanamori and Given, 1982; Fukao, 1995; Brodsky et al., 2003; Ekström and Stark, 2013; Allstadt, 2013). This assumption is justified to the extent that the spatial scale of the slide is small compared to the wavelength of the seismic waves and with the distances to the recording seismic stations. Hence we restrict our analysis to signals with periods longer than 30 s.

The time history of each component (north, east, vertical) was parametrized using a sequence of partially overlapping isosceles triangles. In this study we used 8 triangles, each with a half duration of 10 s. Synthetic seismograms were calculated by summation of Earth's elastic normal modes with corrections for laterally heterogeneous crust and mantle (Ekström, 2011). We solved for the amplitudes of the triangles that

NHESSD

2, 7309–7327, 2014

Seismology of the Oso-Steelhead landslide

C. Hibert et al.

Title Page

Abstract

Introduction

Conclusions

References

Tables

Figures

◀

▶

◀

▶

Back

Close

Full Screen / Esc

Printer-friendly Version

Interactive Discussion



define the time histories of each component of the force by minimizing, in a least-squares sense, the misfit between observed and corresponding synthetic seismograms (Fig. 4a). The time history of each force component was constrained to integrate to zero to satisfy the condition that the sliding mass must be at rest before and after the landslide.

The maximum of the inverted forces is 1.3×10^{10} N and the duration of sliding is approximately 90 s (Fig. 4b). The time-varying displacement $D[t]$ of the center of mass is estimated from double integration of the forces

$$D[t] = -\frac{1}{m} \iint_0^t F[\tau] d\tau. \quad (2)$$

The trajectory is scaled to fit ground observations by adjusting the mass m in Eq. (2), thus also providing an estimate of the mass. The inverted trajectory that best fits the geometry of the departure zone and of the deposits was obtained by using a mass of 1.5×10^{10} kg, and it shows an initial center-of-mass acceleration to the south-east and then a propagation to the south (Fig. 5). The curvature of the trajectory follows well the shape of the maximum accumulation area. We infer a runout distance of 800 m. Assuming a density of the deposits of $2000\text{--}2500$ kg m⁻³, the inferred volume ranges from 6.0×10^6 to 7.5×10^6 m³. This is similar to, but smaller than, the value obtained by an analysis of the total landslide deposits (Keaton et al., 2014).

We infer kinematic parameters from the integration of the inverted forces. The maximum bulk speed reached by the center of mass of the landslide was 19.4 ms⁻¹ and the maximum acceleration was 1.0 ms⁻² (Fig. 4c). The maximum speed, and the associated momentum and kinetic energy, are reached after 35 s after a displacement of approximately 400 m (Fig. 6), which corresponds to the moment when the center of mass reached the break between the slope and the valley (Fig. 5). After this time the center of mass started to decelerate. The total potential energy lost during the slide computed from the drop height inferred from the LFH is about 1.6×10^{13} J. It is almost

Seismology of the Oso-Steelhead landslide

C. Hibert et al.

Title Page

Abstract

Introduction

Conclusions

References

Tables

Figures



Back

Close

Full Screen / Esc

Printer-friendly Version

Interactive Discussion



six times the maximum kinetic energy calculated from the center-of-mass velocity, estimated at 2.8×10^{12} J (Fig. 6a and b).

4 Discussion

4.1 Dynamics of the first event from comparison of the LFH and short-period data

The combined analysis of short-period seismic data with the dynamics inferred from long-period waves provides important information on large landslide motion (Schneider et al., 2010; Yamada et al., 2013; Allstadt, 2013; Hibert et al., 2014). While the long-period waves and the force-history (LFH) inversion provide insight into the temporal evolution of the bulk momentum of the whole landslide mass, the short-period waves reflect spatially complex momentum exchanges across the basal slide area at shorter length scales. Hence short-period signals are sensitive to far more variables, including small-scale relief and topographic obstacles along the runout path, variability in basal friction, and mobility of the granular material within the sliding mass. Strong impulsive bursts of energy in the short-period signals can sometimes be tied to the fall of individual blocks (Huang, 2007) or to the impact of debris after a free-falling phase (Deparis et al., 2008; Dammeier et al., 2011; Hibert et al., 2011).

In order to compare the LFH with the short-period seismic signals, we first computed the travel time of the signal with respect to the origin time given by the LFH inversion. An average propagation velocity can be estimated from comparison of the arrival times recorded at stations JCW and CMW, for which good quality time-picks of the signal onset were possible. We find an average velocity of $\sim 1.1 \text{ km s}^{-1}$. Using this velocity, a shift of 10 s is applied to the LFH to align it with the short-period seismic signal recorded at station JCW. The interpretation that follows is not sensitive to small variations in this assumed propagation velocity.

Title Page

Abstract

Introduction

Conclusions

References

Tables

Figures



Back

Close

Full Screen / Esc

Printer-friendly Version

Interactive Discussion



Seismology of the Oso-Steelhead landslide

C. Hibert et al.

Title Page	
Abstract	Introduction
Conclusions	References
Tables	Figures
◀	▶
◀	▶
Back	Close
Full Screen / Esc	
Printer-friendly Version	
Interactive Discussion	



As Fig. 5 shows, the initial acceleration of the landslide generated very weak short-period seismic waves. Once peak acceleration of the center of mass was reached, a low-amplitude short-period signal emerged from the noise. This timing disparity suggests fragmentation of the initially intact mass while it was already accelerating on the slope (Allstadt, 2013; Hibert et al., 2014). At that point, the magnitude of acceleration along the trajectory started to decrease. The highest amplitudes of the short-period seismic signal occurred at the moment deceleration began. During the whole deceleration phase (inferred from the LFH), the short-period seismic signal amplitude decreased monotonically and passed below the noise level at roughly the same time that the center of mass came to a halt.

4.2 Estimating the dynamics and size of the second event from short-period signals

The seismic signals of the second event are more difficult to interpret. The two amplitude peaks observed (following band-pass filtering at 1–3 Hz; Fig. 3) at approximately 30 and 45 s after the signal onset of the second event are possibly related to the impacts of large chunks of debris with the terrain or with the earlier landslide surface after a free-fall or a very short-lived motion. A composite slope failure process is another possible explanation. These two amplitude peaks are not visible in the 3–10 Hz band. In a previous study (Hibert et al., 2014), we observed that seismic signals produced by the two major landslides during the Bingham Canyon open-pit mine collapse exhibited amplitude peaks that originated in the flowing mass hitting topographical barriers and that were stronger in the 1–3 Hz frequency band than in the 3–10 Hz band. This observation points to a higher sensitivity of the 1–3 Hz frequency band to topographical effects, and prompts the interpretation that the two peaks observed for the second Oso-Steelhead event were generated as sliding and flowing debris encountered topographic obstacles. Multiple time-overlapping breakaways and short phases of motion may explain why no strong long-period waves were generated by the second event.

Seismology of the Oso-Steelhead landslide

C. Hibert et al.

[Title Page](#)[Abstract](#)[Introduction](#)[Conclusions](#)[References](#)[Tables](#)[Figures](#)[◀](#)[▶](#)[◀](#)[▶](#)[Back](#)[Close](#)[Full Screen / Esc](#)[Printer-friendly Version](#)[Interactive Discussion](#)

In the absence of significant long-period seismic waves records for the second event, we are not able to determine its mass and volume using the inversion method presented above. However, the lack of a long-period signal constrains the bulk momentum change of the second event to be much smaller than that of the first. The amplitude of the long-period signal recorded at the closest station (B05D) is approximately three times higher than the noise amplitude. The amplitude of the long-period signal is roughly proportional to the force exerted by the landslide on the earth, and hence to the mass and the acceleration of the center-of-mass of the landslide. If we assume the same peak acceleration for the center-of-mass of both events (Ekström and Stark, 2013), the fact that the amplitude of the long-period seismic signal of the second event is lower than the noise level implies that the mass of the second landslide is at least three times lower than the mass of the first. Consequently, the upper bound for the second landslide mass is roughly 25 % of the total mass mobilized. Note that this upper bound would rise if the center-of-mass peak acceleration of the second landslide were smaller than the first.

Earlier studies (Hibert et al., 2011; Dammeier et al., 2011) have shown that a rough estimate of landslide volume can be deduced from analysis of the seismic energy of the short-period waves, thought to be related to the potential energy released by vertical displacement of the landslide mass. We computed and compared the energy of the seismic signal of the first and second landslides in the 3–10 Hz frequency band. This frequency band is close to that chosen for the events for which this seismic-energy approach has been developed (Hibert et al., 2011; Dammeier et al., 2011). It also has the advantage that it is considered less influenced by topographic effects, as discussed previously. We found a seismic energy ratio between the first and second events of 6.5 at the JCW station. If the ratio of dissipated potential energies is the same as their seismic energy ratio, and if we assume (for the moment) the same run-out distances and the same average sliding angle for both events, the second slope collapse would have a mass approximately 13 % of the total mobilized Oso landslide mass. However, ground observations (Keaton et al., 2014) and the measured duration of short-period

seismic signals suggest that the run-out distance of the second event is shorter than the first, possibly by a factor of two or three, depending on where the departure area of the second landslide is located.

Two possible locations for the departure zone of the second event can be identified (Fig. 5b): (a) at the head scarp, or (b) from the collapsed structure resting at the top of the deposits of the first event. A shorter run-out distance with the same amount of potential energy dissipated would imply that the mass of the second event is bigger, assuming the same angle of sliding. For scenario (a), with a run-out distance half that of the first landslide, the second landslide would represent approximately 20 % of the total collapsed mass. For scenario (b), with a run-out distance for the second landslide a third of the first, the mass of the second collapse would represent 30 % of the total landslide mass. Given the uncertainty over which scenario is correct, we estimate the percentage of the debris mobilized by the second event at between 15 and 30 % of the whole Oso landslide mass. This is in agreement with the ground observations (Keaton et al., 2014) and their volume estimate for the second major failure at around 15 to 50 % of the total.

5 Conclusions

Our analysis of the seismic signals generated by the Oso-Steelhead landslide provides information on its failure sequence together with estimates of key parameters of the landslide dynamics. Two separate events are identified from the seismic data recorded at proximal stations, confirming ground observations of two distinct and substantial slope failures (Keaton et al., 2014). Differences in the seismic features of each event point to variation in their source characteristics and therefore differences in the way runout took place in each case.

The seismic signal of the first event exhibits all the known features of those generated by landslides, with emergent onset, no distinct P and S waves and no clear high-amplitude peak in the higher frequency bands. The strong long-period surface

Seismology of the Oso-Steelhead landslide

C. Hibert et al.

Title Page

Abstract

Introduction

Conclusions

References

Tables

Figures



Back

Close

Full Screen / Esc

Printer-friendly Version

Interactive Discussion



Seismology of the Oso-Steelhead landslide

C. Hibert et al.

Title Page

Abstract

Introduction

Conclusions

References

Tables

Figures

◀

▶

◀

▶

Back

Close

Full Screen / Esc

Printer-friendly Version

Interactive Discussion



waves indicate the mobilization and acceleration of a large landslide mass. Inversion of these long-period surface-waves generates a “landslide-force history” or LFH. The bulk run-out trajectory inferred from this LFH is consistent with ground and remote-sensing observations. Through approximate scaling of the LFH trajectory against these observations, we estimate that the mass of the first landslide is about 1.5×10^{10} kg, corresponding to a volume in the range 6.0×10^6 to 7.5×10^6 m³. The peak center-of-mass velocity and acceleration inferred from the LFH inversion are 19.4 and 1.0 ms⁻² respectively.

The seismic signal of the second event is more impulsive, shows several amplitude peaks, and has little energy at long periods, which makes LFH inversion impossible. While these observations are difficult to interpret in geomorphic terms, recent studies of short-period seismic signals generated by mass movements provide some guidance. They lead us to suspect that the observed signal may have resulted from a complex breakaway sequence that merged into one apparent failure event, with possibly free-fall episodes, followed by a short runout that was abruptly stopped by topographic obstacles. Analysis of the seismic energy of the signal filtered between 3–10 Hz recorded at the JCW station gives a rough estimate of the volume of the second event, at around 15–30 % of the total mobilized volume, in agreement with that estimated from other observations. Based on this estimate and the volume inferred for the first landslide from long-period seismic wave inversion, we deduce the total debris volume mobilized by the Oso-Steelhead events to be between 7×10^6 and 10×10^6 m³, consistent with estimates from ground observations and lidar mapping (Keaton et al., 2014).

Acknowledgements. This work was supported by the US National Science Foundation Division of Earth Sciences and the Geomorphology and Land-use Dynamics/Geophysics programs under award 1227083 and 1148176, and the US National Science Foundation Division of Civil, Mechanical, and Manufacturing Innovation and the Hazards SEES program under award 1331499. We thank the operators of the seismic UU networks for collecting the data used in this study, and the IRIS Data Management System for providing easy access to the data.

References

- Allstadt, K.: Extracting source characteristics and dynamics of the August 2010 Mount Meager landslide from broadband seismograms, *J. Geophys. Res.*, 118, 1472–1490, doi:10.1002/jgrf.20110, 2013. 7311, 7313, 7315, 7316
- 5 Brodsky, E. E., Gordeev, E., and Kanamori, H.: Landslide basal friction as measured by seismic waves, *Geophys. Res. Lett.*, 30, 2236, doi:10.1029/2003GL018485, 2003. 7311, 7313
- Dammeier, F., Moore, J. R., Haslinger, F., and Loew, S.: Characterization of alpine rock-slides using statistical analysis of seismic signals, *J. Geophys. Res.*, 116, F04024, doi:10.1029/2011JF002037, 2011. 7311, 7312, 7315, 7317
- 10 Deparis, J., Jongmans, D., Cotton, F., Baillet, L., Thouvenot, F., and Hantz, D.: Analysis of rock-fall and rock-fall avalanche seismograms in the French Alps, *B. Seismol. Soc. Am.*, 98, 1781–1796, doi:10.1785/0120070082, 2008. 7311, 7312, 7315
- Ekström, G.: A global model of Love and Rayleigh surface wave dispersion and anisotropy, 25–250 s, *Geophys. J. Int.*, 187, 1668–1686, doi:10.1111/j.1365-246X.2011.05225.x, 2011. 7313
- 15 Ekström, G. and Stark, C. P.: Simple scaling of catastrophic landslide dynamics, *Science*, 339, 1416–1419, doi:10.1126/science.1232887, 2013. 7311, 7313, 7317
- Favreau, P., Mangeney, A., Lucas, A., Crosta, G., and Bouchut, F.: Numerical modeling of landquakes, *Geophys. Res. Lett.*, 37, L15305, doi:10.1029/2010GL043512, 2010. 7311
- 20 Fukao, Y.: Single-force representation of earthquakes due to landslides or the collapse of caverns, *Geophys. J. Int.*, 122, 243–248, doi:10.1111/j.1365-246X.1995.tb03551.x, 1995. 7313
- Hibert, C., Mangeney, A., Grandjean, G., and Shapiro, N. M.: Slope instabilities in Dolomieu crater, Réunion Island: from seismic signals to rockfall characteristics, *J. Geophys. Res.*, 116, F04032, doi:10.1029/2011JF002038, 2011. 7311, 7312, 7315, 7317
- 25 Hibert, C., Ekström, G., and Stark, C. P.: Dynamics of the Bingham Canyon Mine landslides from seismic signal analysis, *Geophys. Res. Lett.*, 41, 4535–4541, doi:10.1002/2014GL060592, 2014. 7311, 7315, 7316
- Huang, R.-Q.: Large-scale landslides and their sliding mechanisms in China since the 20th century, *Chinese J. Rock Mech. Eng.*, 26, 433–454, 2007. 7315
- 30 Kanamori, H. and Given, J. W.: Analysis of long-period seismic waves excited by the May 18, 1980, eruption of Mount St. Helens – a terrestrial monopole?, *J. Geophys. Res.*, 87, 5422–5432, doi:10.1029/JB087iB07p05422, 1982. 7313

Seismology of the Oso-Steelhead landslide

C. Hibert et al.

Title Page

Abstract

Introduction

Conclusions

References

Tables

Figures



Back

Close

Full Screen / Esc

Printer-friendly Version

Interactive Discussion



**Seismology of the
Oso-Steelhead
landslide**

C. Hibert et al.

Title Page

Abstract

Introduction

Conclusions

References

Tables

Figures

⏪

⏩

◀

▶

Back

Close

Full Screen / Esc

Printer-friendly Version

Interactive Discussion



- Keaton, J. R., Wartman, J., Anderson, S., Benoît, J., deLaChapelle, J., Gilbert, R., and Montgomery, D. R.: The 22 March 2014 Oso Landslide, Snohomish County, Washington, GEER report, NSF Geotechnical Extreme Events Reconnaissance, http://www.geerassociation.org/GEER_Post_EQ_Reports/Oso_WA_2014/GEER_Oso_Landslide_Report.pdf (last access: December 2014), 172 pp., 2014. 7310, 7311, 7314, 7317, 7318, 7319, 7326
- Moretti, L., Mangeney, A., Capdeville, Y., Stutzmann, E., Huggel, C., Schneider, D., and Bouchut, F.: Numerical modeling of the Mount Steller landslide flow history and of the generated long period seismic waves, *Geophys. Res. Lett.*, 39, L16402, doi:10.1029/2012GL052511, 2012. 7311
- Schneider, D., Bartelt, P., Caplan-Auerbach, J., Christen, M., Huggel, C., and McArdell, B. W.: Insights into rock-ice avalanche dynamics by combined analysis of seismic recordings and a numerical avalanche model, *J. Geophys. Res.*, 115, F04026, doi:10.1029/2010JF001734, 2010. 7311, 7315
- Suriñach, E., Vilajosana, I., Khazaradze, G., Biescas, B., Furdada, G., and Vilaplana, J. M.: Seismic detection and characterization of landslides and other mass movements, *Nat. Hazards Earth Syst. Sci.*, 5, 791–798, doi:10.5194/nhess-5-791-2005, 2005. 7311, 7312
- Vilajosana, I., Suriñach, E., Abellán, A., Khazaradze, G., Garcia, D., and Llosa, J.: Rockfall induced seismic signals: case study in Montserrat, Catalonia, *Nat. Hazards Earth Syst. Sci.*, 8, 805–812, doi:10.5194/nhess-8-805-2008, 2008. 7311
- Yamada, M., Kumagai, H., Matsushi, Y., and Matsuzawa, T.: Dynamic landslide processes revealed by broadband seismic records, *Geophys. Res. Lett.*, 40, 2998–3002, doi:10.1002/grl.50437, 2013. 7311, 7315

Seismology of the Oso-Steelhead landslide

C. Hibert et al.

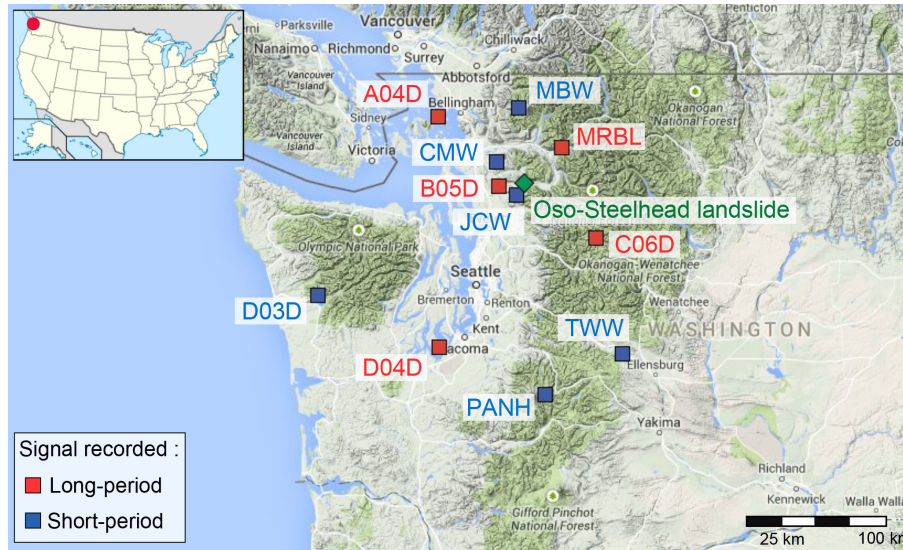


Figure 1. Map of the seismic stations that recorded the short-period (blue square) and/or long-period (red square) seismic waves generated by the Oso-Steelhead landslides (indicated by the green diamond). Stations belong to the Pacific Northwest Regional Seismic Network (CMW, JCW, MBW and TWW), the USArray Transportable Array (A04D, B05D, C06D, D03D and D04D) and the Cascade Chain Volcano Monitoring network (PANH).

Title Page

Abstract

Introduction

Conclusions

References

Tables

Figures



Back

Close

Full Screen / Esc

Printer-friendly Version

Interactive Discussion



Seismology of the Oso-Steelhead landslide

C. Hibert et al.

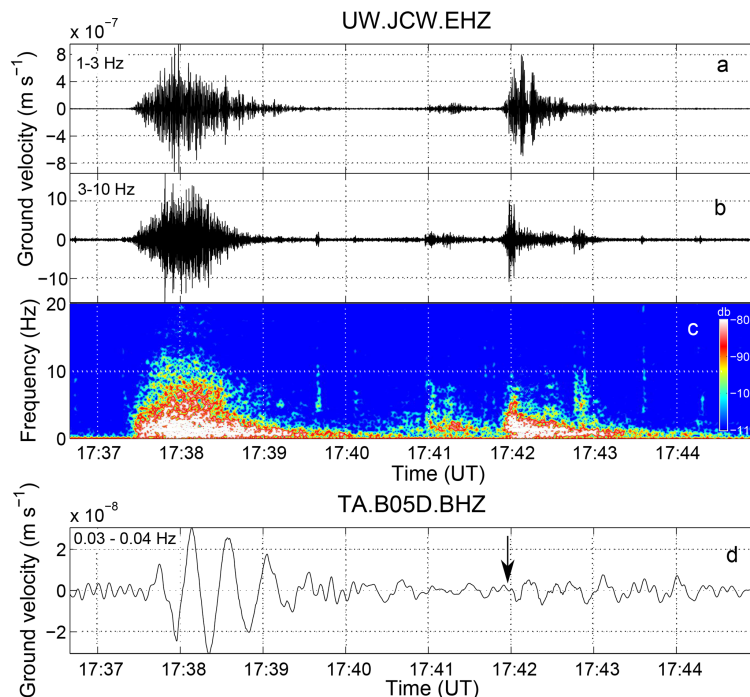


Figure 2. Seismic signal recorded at the short-period station JCW, located 11.7 km from the Oso-Steelhead landslide, filtered between (a) 1–3 Hz and (b) 3–10 Hz. (c) Spectrogram of the seismic signal computed using fast-Fourier transform, with an 8 s moving window and a 90 % overlap. (d) Long-period seismograms recorded at the station B05D and filtered between 0.03 and 0.04 Hz (33–25 s). The black arrow indicates the onset time of the short-period seismic signal generated by the second event.

Seismology of the Oso-Steelhead landslide

C. Hibert et al.

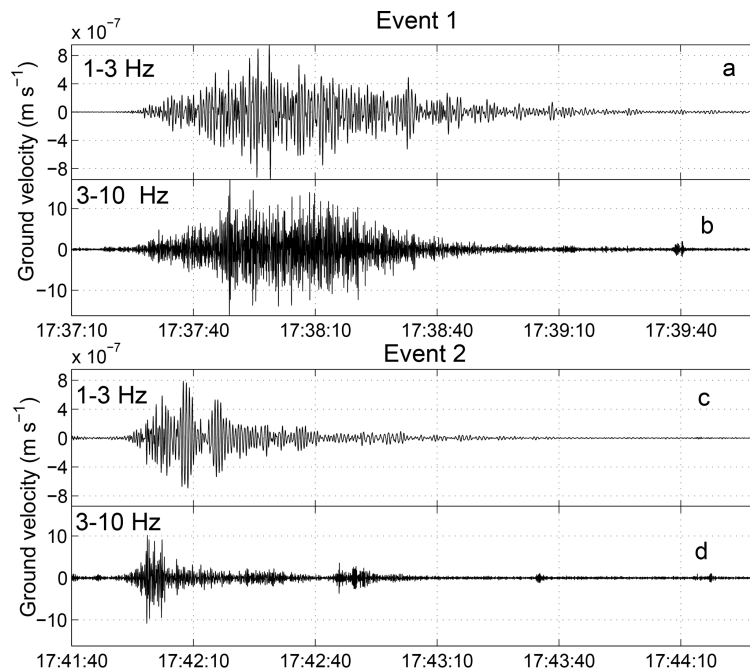


Figure 3. Seismic signals in detail for (a, b) event 1 and (c, d) event 2 at station JCW, filtered between (a, c) 1–3 Hz and (b, d) 3–10 Hz.

[Title Page](#)[Abstract](#)[Introduction](#)[Conclusions](#)[References](#)[Tables](#)[Figures](#)[◀](#)[▶](#)[◀](#)[▶](#)[Back](#)[Close](#)[Full Screen / Esc](#)[Printer-friendly Version](#)[Interactive Discussion](#)

Seismology of the
Oso-Steelhead
landslide

C. Hibert et al.

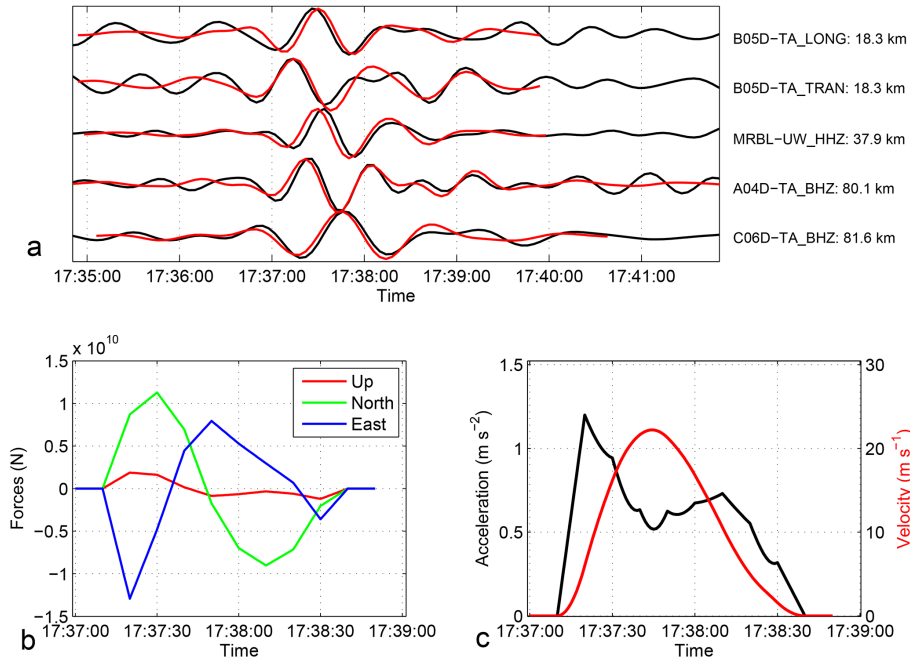


Figure 4. (a) Observed (black) and synthetic (red) long-period seismograms for the first Oso-Steelhead landslide. The station name, component and distance to the landslide are given to the right of each trace. (b) Landslide force histories inverted for the the first Oso-Steelhead landslide. (c) Temporal evolution of the acceleration and the velocity of the center of mass inferred from the integration of the inverted forces.

Title Page

Abstract

Introduction

Conclusions

References

Tables

Figures



Back

Close

Full Screen / Esc

Printer-friendly Version

Interactive Discussion



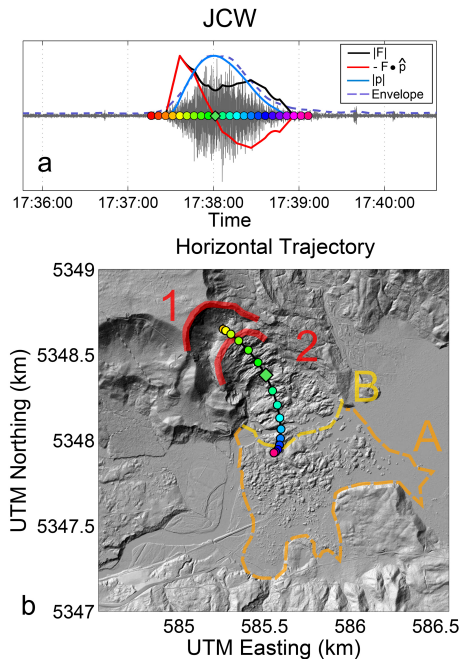


Figure 5. (a) Short-period seismogram at station JCW filtered between 3 and 7 Hz together with the modulus of the inverted forces (black curve), the scalar product of the opposing force F and the normalized moment \hat{p} (red curve), the modulus of the inverted moment (blue curve) and the smoothed envelope. Time t_0 indicates the origin start time of the LFH, before shifting it by the travel-time of the seismic waves. **(b)** Inferred center-of-mass trajectory for the first landslide. Colored dots indicates the time at which the center of mass occupied the corresponding position along the inferred trajectory. The yellow and orange dashed contours labeled A and B indicate the extent of the first and second landslides deposits respectively, identified by Keaton et al. (2014). The red lines labeled 1 and 2 indicate two possible locations for the departure zone of the second landslide.

Seismology of the Oso-Steelhead landslide

C. Hibert et al.

Title Page

Abstract Introduction

Conclusions References

Tables Figures

◀ ▶

◀ ▶

Back Close

Full Screen / Esc

Printer-friendly Version

Interactive Discussion



Seismology of the Oso-Steelhead landslide

C. Hibert et al.

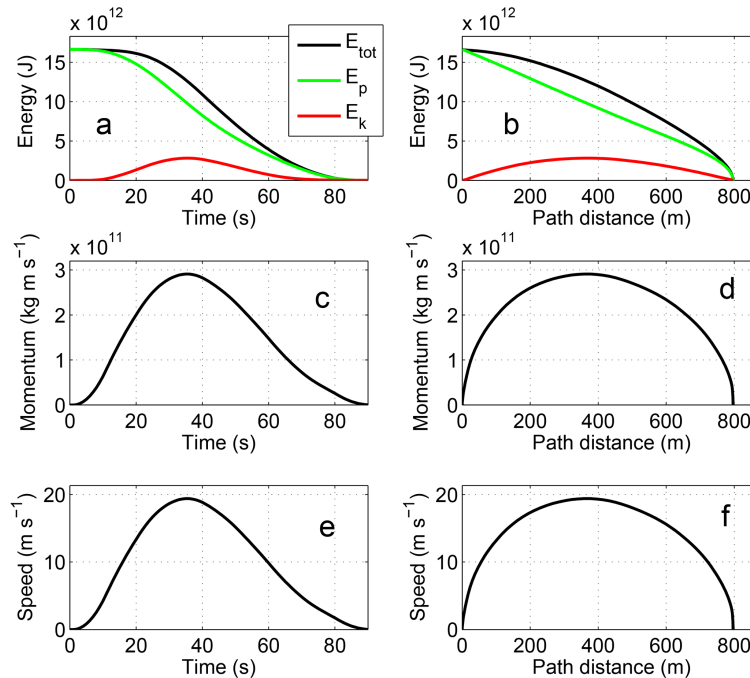


Figure 6. Total energy (black), potential energy (green) and kinetic energy (red) as **(a)** a function of the time and **(b)** a function of the traveled distance. Momentum of the center-of-mass as **(c)** a function of the time and **(d)** a function of traveled distance. Speed of the center-of-mass as **(e)** a function of the time and **(f)** a function of the traveled distance.